

Critical local moment fluctuations and enhanced pairing correlations in a cluster Anderson model

Ang Cai and Qimiao Si

Department of Physics and Astronomy, Rice Center for Quantum Materials, Rice University, Houston, Texas, 77005, USA

J. H. Pixley

*Department of Physics and Astronomy, Center for Materials Theory,
Rutgers University, Piscataway, NJ 08854, USA and*

*Condensed Matter Theory Center and the Joint Quantum Institute,
Department of Physics, University of Maryland, College Park, Maryland 20742-4111, USA*

Kevin Ingersent

Department of Physics, University of Florida, Gainesville, Florida 32611-8440, USA

(Dated: February 25, 2020)

The appearance of unconventional superconductivity near heavy-fermion quantum critical points (QCPs) motivates investigation of pairing correlations close to a “beyond Landau” Kondo-destruction QCP. We focus on a two-Anderson-impurity cluster in which Kondo destruction is induced by a pseudogap in the conduction-electron density of states. Analysis via continuous-time quantum Monte-Carlo and the numerical renormalization group reveals a previously unstudied QCP that both displays the critical-local moment fluctuations characteristic of Kondo destruction and leads to a strongly enhanced singlet-pairing susceptibility. Our results provide new insights into the mechanism for superconductivity in quantum critical metals.

PACS numbers: 71.10.Hf, 71.27.+a, 74.40.Kb, 74.70.Tx, 75.20.Hr

I. INTRODUCTION

Heavy-fermion metals are highly tunable and provide a prototype setting to explore strong correlation physics in general¹⁻³. In heavy-fermion systems, unconventional superconductivity often develops near their quantum critical points (QCPs)^{4,5}. Detailed theoretical and experimental studies have provided evidence for different classes of QCP. One class follows the Landau theory, in which criticality is dictated by the fluctuations of an order parameter⁶⁻⁸. Another class of QCP goes beyond the Landau framework, in that it involves new critical modes besides order-parameter fluctuations. The additional critical modes describe a critical destruction of the Kondo entanglement between the localized magnetic moments and conduction electrons^{9,10}, which is a form of electronic localization-delocalization instability. As such, studies of superconducting pairing driven by Kondo-destruction quantum criticality elucidate unconventional superconductivity not only in heavy-fermion metals but also in a broad range of other correlated electron systems.

An important example of a Kondo-destruction QCP occurs in CeRhIn₅, which has the highest T_c among all the Ce-based heavy-fermion superconductors¹¹⁻¹⁴ and is generally believed to have a $d_{x^2-y^2}$ pairing symmetry. A sudden change of the Fermi-surface size across the antiferromagnetic QCP in CeRhIn₅, accompanied by a diverging tendency of the carrier effective mass¹⁵, defy explanation within the Landau-based (spin-density-wave) scenario but instead provide evidence supporting the Kondo-destruction picture.

How unconventional superconductivity arises near a Kondo-destruction QCP has yet to receive systematic theoretical study. The question is challenging because the normal state is a non-Fermi liquid with quasiparticles turned critical. An avenue has been opened by the development of a cluster extended dynamical mean-field theory (C-EDMFT)²¹, which maps the periodic Anderson model onto a cluster model coupled to self-consistently determined fermionic and bosonic baths, where the latter decohere and eventually destroy the Kondo entanglement²². The Kondo destruction QCP of the lattice problem is embedded in the QCP of the quantum cluster model, and the multi-site cluster allows the development of unconventional pairing.

It is illuminating to study the quantum cluster model by itself. Previous studies¹⁶⁻²⁰ demonstrate that quantum impurity models can manifest hallmarks of a Kondo-destruction QCP such as a vanishing Kondo energy scale, ω/T scaling of the dynamics, and a fractional exponent in the temperature dependence of the local spin susceptibility. This is largely due to the fact that Kondo destruction is primarily a local phenomenon, and the neglect of spatial correlation is relatively unimportant. Recent work in an Ising-anisotropic cluster Bose-Fermi Anderson model²³ has found enhanced pairing correlations near the Kondo-destruction QCP. This finding raises an important question: Does Kondo-destruction quantum criticality robustly promote superconducting pairing correlations?

This work investigates a two-impurity pseudogap Anderson model with Ising exchange between the impurity spins. We show that the model exhibits a Kondo-

destruction QCP that has not been discussed in previous publications. Instead of the coupling to a bosonic bath that was responsible for Kondo destruction in Ref. 23, here the driving force is exchange coupling of the impurity spins to a conduction band with a density of states that vanishes in power-law fashion at the Fermi energy²⁴. The presence of a different mechanism for Kondo destruction allows us to address the generality with which this type of quantum criticality promotes superconducting pairing.

II. MODEL AND SOLUTION METHODS

The two-impurity Ising-anisotropic Anderson Hamiltonian is

$$H = \sum_{\mathbf{k}, \sigma} \epsilon_{\mathbf{k}} c_{\mathbf{k}\sigma}^\dagger c_{\mathbf{k}\sigma} + \frac{V}{\sqrt{N_k}} \sum_{\mathbf{k}, j, \sigma} (e^{i\mathbf{k}\cdot\mathbf{r}_j} d_{j\sigma}^\dagger c_{\mathbf{k}\sigma} + H.c.) + \epsilon_d \sum_{j, \sigma} d_{j\sigma}^\dagger d_{j\sigma} + U \sum_j n_{j\uparrow} n_{j\downarrow} + I_z S_1^z S_2^z, \quad (1)$$

with $\epsilon_{\mathbf{k}}$ being the conduction-electron dispersion, V the hybridization (assumed to be local), N_k the number of unit cells in the host, ϵ_d the impurity level energy, U the on-site repulsion, and I_z the Ising exchange coupling between impurities at positions \mathbf{r}_j ($j = 1, 2$); $n_{j\sigma} = d_{j\sigma}^\dagger d_{j\sigma}$ for $\sigma = \uparrow, \downarrow$, and $S_j^z = \frac{1}{2}(n_{j\uparrow} - n_{j\downarrow})$. The conduction-band density of states is chosen to be

$$\rho(\epsilon) = \frac{1}{N_k} \sum_{\mathbf{k}} \delta(\epsilon - \epsilon_{\mathbf{k}}) = \rho_0 |\epsilon/D|^r \Theta(D - |\epsilon|), \quad (2)$$

where D is the half-bandwidth. For $r > 0$, $\rho(\epsilon)$ has a pseudogap at the Fermi energy ($\epsilon = 0$). The impurity-band coupling is fixed by $\Gamma(\epsilon) = \pi \sum_{\mathbf{k}} V^2 \delta(\epsilon - \epsilon_{\mathbf{k}}) = \Gamma_0 |\epsilon/D|^r$, the hybridization function with $\Gamma_0 = \pi \rho_0 V^2$.

For simplicity, we consider only the particle-hole-symmetric case $\epsilon_d = -U/2$ and take the limit of infinite separation $|\mathbf{r}_1 - \mathbf{r}_2|$ in which there is a vanishing hybridization-induced Ruderman-Kittel-Kasuya-Yosida interaction and the two impurities are coupled only via the Ising exchange I_z . With $I_z = 0$, we have two independent one-impurity pseudogap models; for $0 < r < \frac{1}{2}$, a Kondo-destruction QCP^{25,26} that we denote CR1 separates a Kondo phase ($\Gamma_0 > \Gamma_c$) from a local-moment phase ($\Gamma_0 < \Gamma_c$). With $\Gamma_0 = 0$ and $I_z > 0$, the two impurity spins are decoupled from the conduction band and anti-align in an Ising antiferromagnetic configuration. Our goal is to probe the quantum phase transitions that arise when both $\Gamma_0 > 0$ and $I_z > 0$ ²⁷.

We begin by analyzing the perturbative effect of the coupling I_z near the single-impurity critical point CR1. At this QCP, $\langle S_i^z(\tau) S_j^z \rangle \sim \tau^{-(1-x_1)}$, with x_1 being an r -dependent exponent that satisfies $0 < x_1(r) < 1$ ¹⁹. Since the impurities decouple, $\langle S_1^z(\tau) S_2^z(\tau) S_1^z S_2^z \rangle \sim \tau^{-2(1-x_1)}$. The scaling dimension of $S_1^z S_2^z$ is thus seen to be $1 - x_1(r)$ and we obtain the scaling dimension $[I_z] = x_1(r)$. The

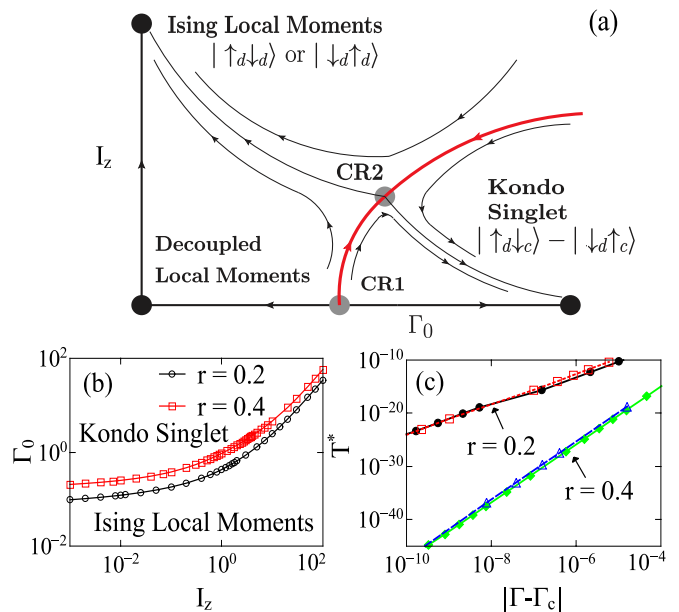


FIG. 1: (a) Conjectured RG flow of the symmetric two-impurity pseudogap Anderson model. Gray dots represent unstable fixed points and black dots represent stable fixed points. CR1 is the unstable fixed point of the single-impurity pseudogap Anderson model. CR2 is the unstable fixed point of the two-impurity model studied in this work. The red line marks the separatrix and phase boundary. (b) Phase boundary of the symmetric two-impurity pseudogap Anderson model on the I_z - Γ_0 plane for $r = 0.2$, $U = -2\epsilon_d = 0.3$ and for $r = 0.4$, $U = -2\epsilon_d = 0.1$. The boundary value of Γ_0 obtained from NRG calculations is plotted before extrapolation to the continuum limit (see discussion in Appendix A). (c) Crossover scale T^* from the NRG vs $|\Gamma_0 - \Gamma_c|$ on both sides of the phase boundary for $r = 0.2$, $I_z = 1.54$, $\Gamma_c \simeq 0.5503$ and for $r = 0.4$, $I_z = 0.73$, $\Gamma_c \simeq 0.8032$. Filled symbols represent $\Gamma > \Gamma_c$ and open symbols represent $\Gamma < \Gamma_c$. Fits to $T^* \propto |\Gamma_0 - \Gamma_c|^\nu$ yield estimated exponents given in the text.

Hamiltonian term $I_z S_1^z S_2^z$ is therefore a relevant perturbation at CR1 and will likely lead the two-impurity model to a new unstable fixed point CR2 as shown on a conjectured RG flow diagram in Fig. 1(a).

Since the pseudogap breaks conformal invariance, the model (1) cannot be treated nonperturbatively using conventional analytical methods²⁸⁻³⁰ and we instead employ continuous-time quantum Monte-Carlo (CT-QMC)^{31,32} and the numerical renormalization group (NRG)^{33,34}. We present results for two representative cases: (i) $r = 0.2$, $U = 0.3$ and (ii) $r = 0.4$, $U = 0.1$, where we have set the energy scale $D = 1$. In CT-QMC calculations we vary I_z at fixed Γ_0 , and are able to reach sufficiently low temperatures to access the asymptotic quantum critical regime. We fix I_z and vary Γ_0 when applying the NRG, a technique that can reach arbitrarily close to absolute zero but has limited ability to calculate finite-temperature dynamics. Further numerical details are described in Appendix A.

III. QUANTUM CRITICAL PROPERTIES

A critical phase boundary can be mapped out within the NRG by looking for the hybridization width $\Gamma_c(I_z)$ at which the asymptotic low-energy many-body spectrum jumps from that of one stable fixed point to another. The phase boundaries are plotted Fig. 1(b). For Γ_0 close to Γ_c , the NRG spectrum flows away from the critical spectrum toward one or other of the stable fixed points around a crossover temperature $T^* \propto |\Gamma_0 - \Gamma_c|^\nu$. Using this relation, illustrated in Fig. 1(c), one obtains $\nu^{-1} = 0.334(2)$ for $r = 0.2$ and $\nu^{-1} = 0.1835(4)$ for $r = 0.4$.

To search for a QCP using CT-QMC, we examine the Binder ratio³⁵ $B(\beta, I_z) = \langle M^4 \rangle / \langle M^2 \rangle^2$, where the staggered impurity magnetization $M = \beta^{-1} \int_0^\beta d\tau [S_1^z(\tau) - S_2^z(\tau)]$. Plots of $B(\beta, I_z)$ vs I_z for different values of $\beta = 1/k_B T$ should all cross at the location $I_z = I_c$ of a QCP, as is indeed shown in Fig. 2(a) for $r = 0.2$ and Fig. 2(b) for $r = 0.4$. A scaling collapse

$$B(\beta, I_z) = f(\beta^{1/\nu}(I_z - I_c)/I_c + C\beta^{-\phi/\nu}) \quad (3)$$

(where the term involving C accounts for sub-leading finite temperature corrections) demonstrates that the quantum phase transition at $I_z = I_c$ is second order, as illustrated in Fig. 2(c). By minimizing a quality function³⁶ (see Appendix B for details), we find $\nu^{-1} = 0.33(4)$ for $r = 0.2$ and $\nu^{-1} = 0.20(2)$ for $r = 0.4$, reproducing the NRG values to within estimated errors³⁷.

The static staggered local spin susceptibility (the order-parameter susceptibility), defined as $\chi_z = \beta \langle M^2 \rangle$, diverges at the QCP as

$$\chi_z(I_z = I_c, T) \sim T^{-x}, \quad (4)$$

as seen in Fig. 2(d). The values of $x(r)$ from CT-QMC [$x(0.2) = 0.78(4)$ and $x(0.4) = 0.34(5)$] and the NRG [$x(0.2) = 0.78588(3)$ and $x(0.4) = 0.35075(3)$] are in good agreement. We have also calculated the connected spin susceptibility, $\chi_z^c = \beta(\langle M^2 \rangle - \langle |M| \rangle^2)$, which based on the scaling hypothesis can be described by $\chi_z^c(\beta, I_z) = \beta^x g(\beta^{1/\nu}(I_z - I_c)/I_c + C\beta^{-\phi/\nu})$; see Fig. 5 in Appendix C.

We summarize our results for the critical exponents ν^{-1} and x at the two-impurity pseudogap QCP CR2 in Table I, where we have also included NRG values of the order-parameter critical exponent β' defined through $M(\Gamma_0, T = 0, h = 0) \propto (\Gamma_c - \Gamma_0)^{\beta'}$ and the magnetic critical exponent $1/\delta$ defined through $M(\Gamma_0 = \Gamma_c, T = 0, h) \propto |h|^{1/\delta}$, h being an external field that couples solely to the staggered impurity spin (see Fig. 10 in Appendix D). These exponents take values different from those at the single-impurity pseudogap QCP CR1¹⁹, demonstrating CR2 to be a distinct critical point. Moreover, they obey scaling relations $\delta^{-1} = (1 - x)/(1 + x)$ and $\nu^{-1} = (1 - x)/2\beta'$ characteristic of an interacting critical point¹⁹.

We turn to the dynamical properties at CR2 of the single-particle Green's function $G_{i,\sigma}(\tau, T) =$

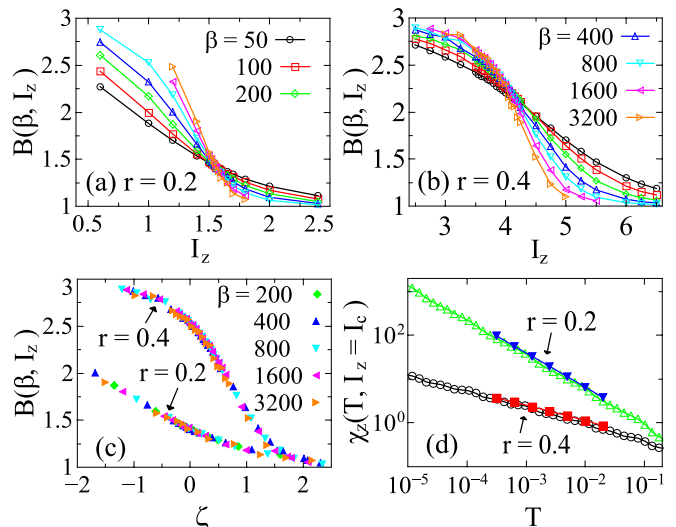


FIG. 2: (a,b) Binder ratio $B(\beta, I_z)$ from CT-QMC vs I_z at various inverse temperatures β for (a) $r = 0.2$, $\Gamma_0 = 0.5$ and (b) $r = 0.4$, $\Gamma_0 = 1.5$. (c) Scaling collapses of $B(\beta, I_z)$ with respect to $\zeta = \beta^{1/\nu}(I_z - I_c)/I_c + C\beta^{-\phi/\nu}$ giving $I_c = 1.56(7)$, $\nu^{-1} = 0.33(4)$ at $r = 0.2$ and $I_c = 3.75(7)$, $\nu^{-1} = 0.20(2)$ at $r = 0.4$. (d) Static staggered local spin susceptibility χ_z vs T at the estimated location $I_z = I_c$ of the QCP, calculated using CT-QMC (filled symbols) and the NRG (open symbols). Fitting to Eq. (4) yields the values of x given in the text.

$\langle T_\tau d_{i,\sigma}^\dagger(\tau) d_{i,\sigma} \rangle$ and the spin correlation function $\chi_z(\tau, T) = \langle T_\tau [S_1^z(\tau) - S_2^z(\tau)](S_1^z - S_2^z) \rangle$. Guided by previous work on the single-impurity models^{16–18,20}, we find from CT-QMC (see Fig. 6 in Appendix C) that these functions share similar power-law forms in the low- T , large- τ limit:

$$G_{i,\sigma}(\tau, T) \sim [\pi T / \sin(\pi \tau T)]^{\eta_G(r)}, \quad (5)$$

$$\chi_z(\tau, T) \sim [\pi T / \sin(\pi \tau T)]^{\eta_\chi(r)}, \quad (6)$$

with exponents $\eta_G(0.2) = 0.795$, $\eta_G(0.4) = 0.600$, $\eta_\chi(0.2) = 0.213$, and $\eta_\chi(0.4) = 0.657$. As expected, $\eta_\chi = 1 - x$ is satisfied within numerical accuracy. Moreover, our results suggest that (i) the relation $\eta_G = 1 - r$ known to hold at CR1³⁸ also applies at CR2, and (ii) $0 < \eta_G < 1$ and $0 < \eta_\chi < 1$, so $G_{i,\sigma}$ and χ_z will also obey ω/T scaling on the real frequency axis²⁰. This supports the interacting nature of CR2.

r	source	$1/\nu$	x	β'	$1/\delta$
0.2	CT-QMC	0.33(4)	0.78(4)		
	NRG	0.334(2)	0.78588(3)	0.31991(2)	0.11990(4)
0.4	CT-QMC	0.20(2)	0.34(5)		
	NRG	0.1835(4)	0.35075(3)	1.7701(2)	0.48066(4)

TABLE I: Critical exponents (defined in the text) at the two-impurity pseudogap QCP CR2. Parentheses enclose the estimated error in the last decimal place.

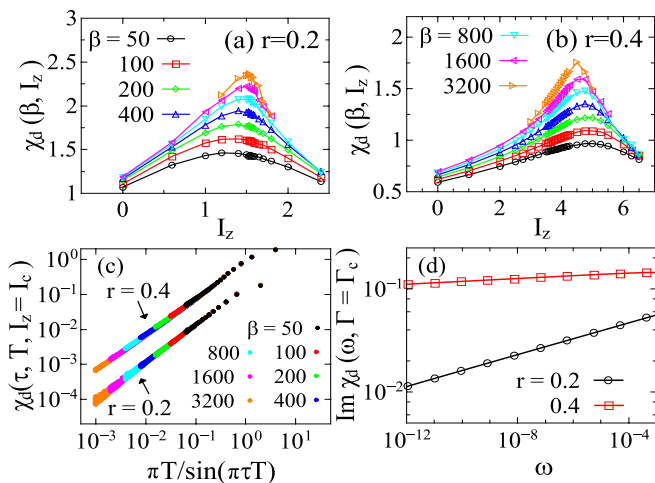


FIG. 3: Singlet pairing susceptibility: (a,b) Static susceptibility $\chi_d(\beta, I_z)$ vs I_z at various inverse temperatures β for (a) $r = 0.2$, $\Gamma_0 = 0.5$, and (b) $r = 0.4$, $\Gamma_0 = 1.5$. (c) Imaginary-time susceptibility $\chi_d(\beta, \tau)$ at $I_z = I_c$, consistent with a $1/\tau^{1+y}$ decay with $y = 0.075$ for $r = 0.2$, $\Gamma_0 = 0.5$ and $y = 0.012$ for $r = 0.4$, $\Gamma_0 = 1.5$. For clarity, the $r = 0.4$ susceptibilities have been multiplied by a factor of 10. (d) NRG results for the imaginary part of the real-frequency susceptibility, $\text{Im} \chi_d(\omega) \propto \omega^y$, at $\Gamma_0 = \Gamma_c$, $T = 0$, calculated both for $r = 0.2$, $I_z = 1.54$ yielding $y = 0.077(1)$ and for $r = 0.4$, $I_z = 0.73$ yielding $y = 0.0139(1)$.

IV. PAIRING SUSCEPTIBILITIES

We study static pairing susceptibilities $\chi_\alpha(\beta, I_z) = \int_0^\beta d\tau \langle T_\tau \Delta_\alpha^\dagger(\tau) \Delta_\alpha \rangle$ with $\Delta_d = (d_{2\downarrow}d_{1\uparrow} - d_{2\uparrow}d_{1\downarrow})/\sqrt{2}$ (singlet channel)³⁹ and $\Delta_p = (d_{1\uparrow}d_{2\uparrow} + d_{1\downarrow}d_{2\downarrow})/\sqrt{2}$ (triplet channel). Using the general four-point correlation function formula in CT-QMC⁴⁰, we find singlet pairing to be significantly enhanced near the QCP, as shown in Figs. 3(a) and 3(b). By contrast, triplet pairing is monotonically suppressed as I_z increases (see Fig. 7 in Appendix C).

At $T = 0$, the imaginary part of the dynamical pairing susceptibility $\text{Im} \chi_d(\omega)$ can be calculated using the NRG. We plot data for $\Gamma_0 = \Gamma_c(I_z)$ in Fig. 3(d) and for other cases in Fig. 11 in Appendix D. Our results can be summarized in the form

$$\text{Im} \chi_d(\omega) \text{sgn}(\omega) \propto \begin{cases} \left| \frac{\omega^*}{D} \right|^y \left| \frac{\omega}{\omega^*} \right|^{1-2r} & |\omega| < \omega^*, I_z < I_c \\ \left| \frac{\omega^*}{D} \right|^y \left| \frac{\omega}{\omega^*} \right|^{1+2r} & |\omega| < \omega^*, I_z > I_c \\ \left| \frac{\omega}{D} \right|^y & \omega^* < |\omega| < \omega_1, \end{cases} \quad (7)$$

where ω_1 is the high-energy scale marking the upper bound of the quantum critical regime and $\omega^* \simeq T^*$ is the scale for crossover into the low-temperature phase. This implies that at the critical point, $\chi_d(\tau) \sim 1/\tau^{1+y}$, cf. Fig. 3(c). The NRG gives $y = 0.077(1)$ for $r = 0.2$ and $y = 0.0139(1)$ for $r = 0.4$, values that agree very well with the CT-QMC estimates of $y = 0.075$ and $y = 0.012$, respectively. Equation (7) also implies (see Appendix E

for derivation) that near the QCP,

$$\text{Re} \chi_d(\omega = 0) = C_1(r) - C_2(r) \left(\frac{1}{y} - \frac{1}{1 \pm 2r} \right) \times \left(\frac{|I_z - I_c|/I_c^\nu}{D} \right)^y \quad (8)$$

with \pm corresponding to $I_z > I_c$ or $I_z < I_c$, and $C_1(r)$ and $C_2(r)$ being independent of I_z . Given that $y\nu \ll 1$, $\text{Re} \chi_d(\omega = 0)$ should have a pronounced cusp at $I_z = I_c$, as confirmed by the numerical data in Figs. 3(a) and 3(b).

V. DISCUSSION AND SUMMARY

We note that, in the single-impurity pseudogap Anderson model, the impurity spectral function vanishes (diverges) as $|\omega|^r$ ($|\omega|^{-r}$) in the local-moment (Kondo-screened) phase²⁵. Our calculations suggest that this property also holds in the present model (see Fig. 8 in Appendix B). This indicates that the frequency dependences of $\text{Im} \chi_d(\omega)$ at the two stable fixed points do not acquire any singular correction²⁶. By contrast, at CR2 the $|\omega|^y$ dependence reflects the relevance of vertex corrections at an interacting critical point. Since CR1 and CR2 both exist only for $0 < r < \frac{1}{2}$, we expect that y is always smaller than $1 \pm 2r$, namely that pairing fluctuations are always strongest in the quantum critical regime, and that as $r \rightarrow \frac{1}{2}$, y and $1 - 2r$ both approach 0 before CR1 and CR2 merge with the Kondo-singlet fixed point and disappear. We therefore conclude that the underlying Kondo-destruction QCP promotes singlet superconducting pairing.

To summarize, we have found a quantum critical point in the two-impurity Anderson model with a pseudogap density of states. It exhibits critical Kondo destruction and shows all the hallmarks of an interacting fixed point, such as hyperscaling relations among critical exponents and ω/T scaling in the dynamical properties. The singlet pairing susceptibility is found to be sharply peaked at the quantum critical point. Our results suggest that Kondo-destruction quantum criticality promotes spin-singlet unconventional superconductivity in a robust way and, as such, is a viable mechanism for understanding superconductivity in CeRhIn₅ and related quantum critical heavy-fermion systems.

Acknowledgements. We acknowledge useful discussions with Y. Chou, S. Kirchner, E. M. Nica, Z. Wang, and H. Xie, as well as technical support from the Center for Research Computing at Rice University. This work was supported in part by NSF Grant No. DMR-1920740 and the Robert A. Welch Foundation Grant No. C-1411 (A.C. and Q.S.), by JQI-NSF-PFC, LPS-MPO-CMTC and Microsoft Q (J.H.P.), and by NSF Grant No. DMR-1508122 (K.I.). The computation was performed through the Extreme Science and Engineering Discovery Environment (XSEDE) under the support of the NSF Grant No. DMR170109, and on the Shared Computing Infrastructure funded by NSF under grant OCI-0959097, NIH

award NCRR S10RR02950, and an IBM Shared University Research (SUR) Award in partnership with CISCO, Qlogic and Adaptive Computing, and Rice University.

Appendix A: Methods

The CT-QMC hybridization expansion algorithm allows us to stochastically sample the perturbation series in the hybridization term free of any sign problem in the infinite separation limit. The average perturbation order exceeds 10^3 per orbital for the largest inverse temperature, $\beta = 3200$ at $\Gamma_0 = 1.5$. Within our specific case, we find the auto-correlation time measured in terms of successful updates will grow not only as temperature is lowered and perturbation order increases, but also as one increases I_z deep into the magnetic ordered phase, where a domain wall like structure can form in the imaginary time direction. Therefore, we have introduced an additional global update in addition to the standard local one kink (a kink refers to a creation and annihilation operator pair) and two kinks update, by exchanging all the kinks between different orbitals within a imaginary time interval of length around $\beta/2$ (with a probability that satisfies detailed balance), to prevent the sampling process from getting trapped in some meta-stable state.

The NRG runs were performed for Wilson discretization parameter $\Lambda = 9$, retaining between 1000 and 4000 many-body eigenstates after each iteration. The Wilsonian discretization of the conduction band reduces the effective density of states so it is appropriate to compare NRG calculations for hybridization width Γ_0 with continuum-limit ($\Lambda \rightarrow 1$) results for hybridization width $\Gamma_0/A(\Lambda, r)$, where $A(\Lambda, r)$ is defined in Ref. 21 of the main text. Hybridization widths reported in the text are the values entered into the NRG calculations and do not include the discretization correction factor.

Appendix B: Finite size scaling of Binder cumulant

The value of ν^{-1} and I_c is determined through minimization of the quality function $S(I_c, \nu^{-1})$, which is essentially the mean square deviation of the scaled data points with respect to the unknown universal function. For k sets of data points represented by $\{x_{ij}, y_{ij}\}$, where $i = 1, \dots, k$ labels different β and j labels different I_z , we define $S(I_c, \nu^{-1}) = 1/N \sum_{i,j} (y_{ij} - Y_{ij})^2$. Here Y_{ij} is the estimated value of the universal function at x_{ij} by linear interpolation from the rest of sets $\{x_{i'j}, y_{i'j}\}$, $i' \neq i$. During the scaling collapse, we start by including all the sets, and then gradually excluding the highest temperature data until the result reaches convergence. Only data points satisfying $\beta^{1/\nu}(I_z - I_c)/I_c \lesssim 1$ are included. The best estimate of I_c and ν^{-1} is where $S(I_c, \nu^{-1})$ reaches its minimum S_{min} . We estimate the error by requiring $S(I_c + \delta I_c, \nu^{-1} + \delta \nu^{-1}) - S_{min} \simeq S_{min}/2$.

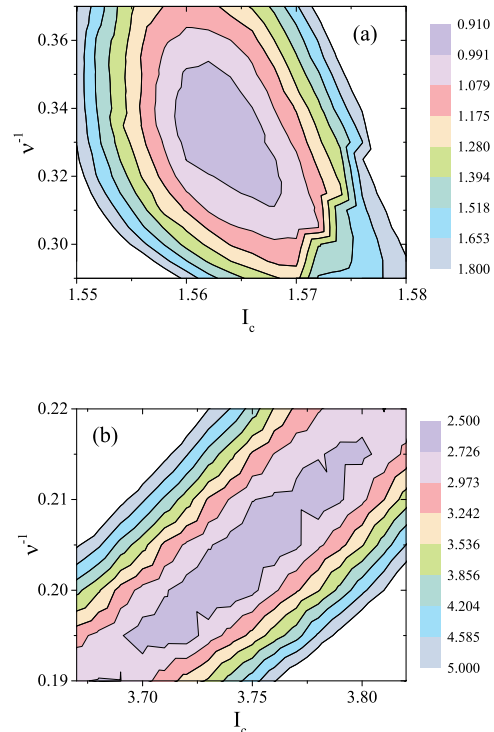


FIG. 4: Contour plot of quality function $S(I_c, \nu^{-1}) \times 10^4$ for the scaling collapse shown in Fig. 2(c) for (a) $r = 0.2$ and (b) $r = 0.4$.

Appendix C: Additional data from CT-QMC

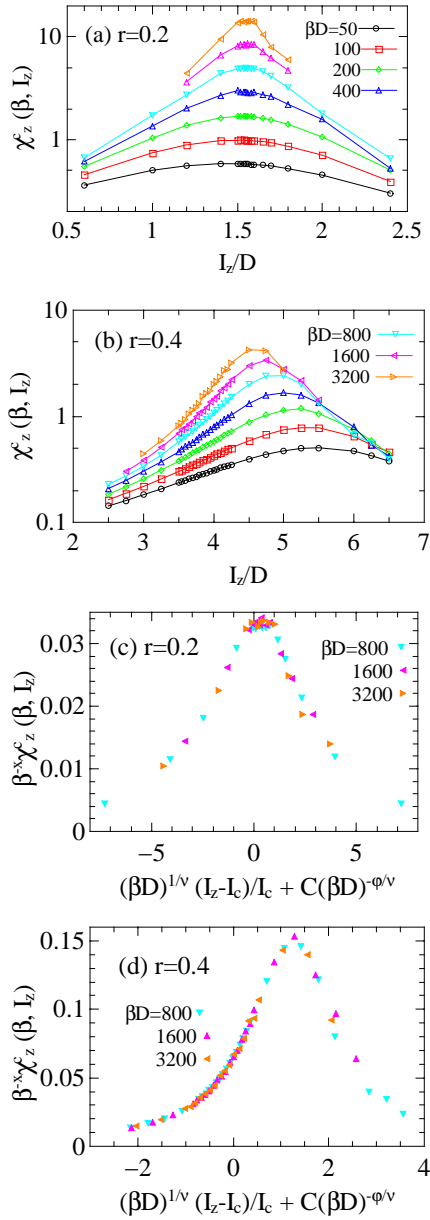


FIG. 5: Connected static staggered spin susceptibility $\chi_z^c(\beta, I_z)$ vs I_z at various inverse temperatures β for (a) $r = 0.2$, $\Gamma_0 = 0.5$ and (b) $r = 0.4$, $\Gamma_0 = 1.5$. (c)(d) Scaling collapse of $\chi_z^c(\beta, I_z)$ in (a) and (b) respectively, with $I_c = 1.53(6)$, $\nu^{-1} = 0.37(8)$, $x = 0.75(4)$ at $r = 0.2$ and $I_c = 4.0(2)$, $\nu^{-1} = 0.26(4)$, $x = 0.42(7)$ at $r = 0.4$. The deviation from exponents in Table I can be attributed to stronger finite-size corrections to χ_z^c .

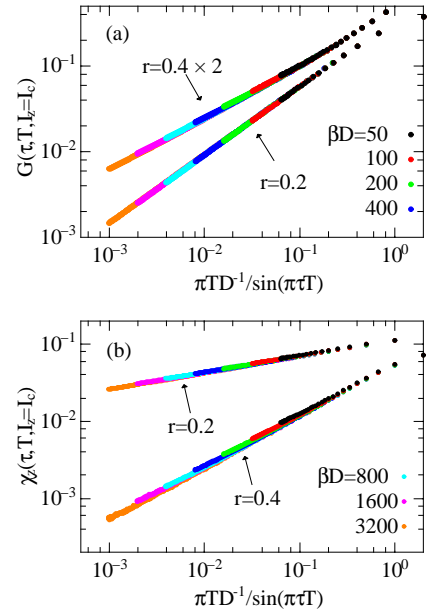


FIG. 6: (a) Scaling of the single-particle Green's function $G(\tau, T, I_z = I_c)$ (averaged over impurity site and spin) with $\pi T / \sin(\pi \tau T)$. We find $G(\tau \rightarrow \infty, T \rightarrow 0, I_z = I_c) \sim [\pi T / \sin(\pi \tau T)]^{\eta_G(r)}$ with $\eta_G(0.2) = 0.795$ and $\eta_G(0.4) = 0.600$, consistent with $\eta_G = 1 - r$ (b) Scaling of the staggered spin correlation function $\chi_z(\tau, T, I_z = I_c)$ with $\pi T / \sin(\pi \tau T)$. We find $\chi_z(\tau \rightarrow \infty, T \rightarrow 0, I_z = I_c) \sim [\pi T / \sin(\pi \tau T)]^{\eta_\chi(r)}$ with $\eta_\chi(0.2) = 0.213$ and $\eta_\chi(0.4) = 0.657$, consistent with $\eta_\chi = 1 - x$. Calculations are performed at $\Gamma_0 = 0.5$ at $r = 0.2$ and $\Gamma_0 = 1.5$ at $r = 0.4$.

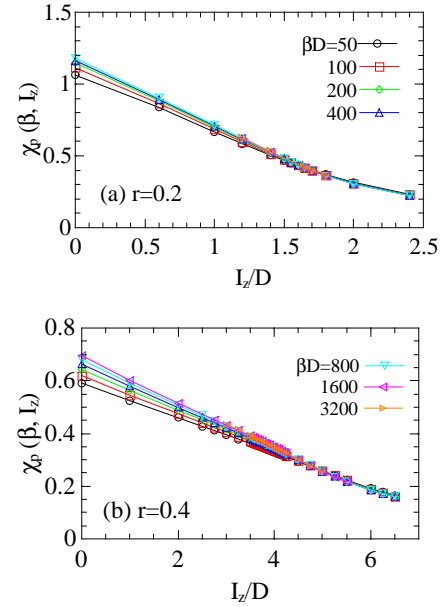


FIG. 7: Static triplet pairing susceptibility $\chi_p(\beta, I_z)$ vs I_z at various inverse temperatures β for (a) $r = 0.2$, $\Gamma_0 = 0.5$ and (b) $r = 0.4$, $\Gamma_0 = 1.5$.

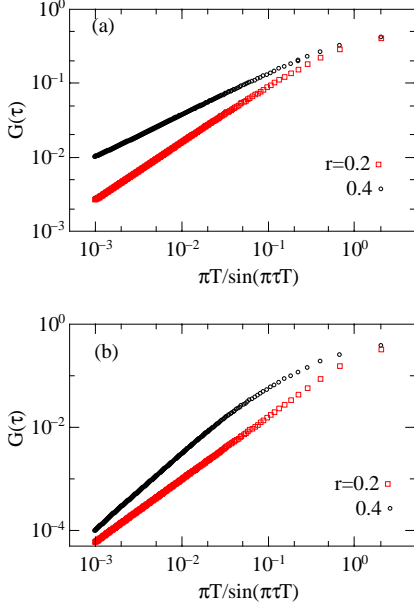


FIG. 8: Single-impurity Green's function $G(\tau)$ at $\beta = 3200$ in (a) the Kondo-screened phase ($I_z = 0$, $\Gamma_0 = 0.5$ for both $r = 0.2$ and $r = 0.4$) and (b) the local-moment phase ($I_z = 3$, $\Gamma_0 = 0.5$ for $r = 0.2$ and $I_z = 2$, $\Gamma_0 = 0.5$ for $r = 0.4$). Fitting to $G_{i,\sigma}(\tau) \sim [\pi T / \sin(\pi\tau T)]^{\eta_G(r)}$ in (a) gives $\eta_G(0.2) = 0.77$ and $\eta_G(0.4) = 0.57$, while in (b) gives $\eta_G(0.2) = 1.21$ and $\eta_G(0.4) = 1.45$. Results are consistent with $G(\tau) \sim 1/\tau^{1\pm r}$ for $I_z > I_c$ or $I_z < I_c$.

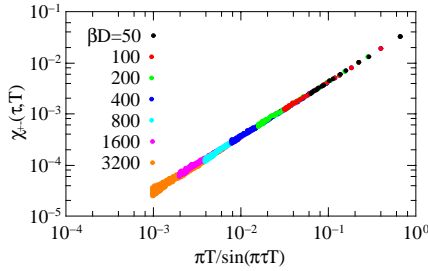


FIG. 9: Transverse component of the staggered spin susceptibility $\chi_{+-}(\tau)$ at $I_z = I_c$, $\Gamma_0 = 0.5$ for $r = 0.2$. $\chi_{+-}(\tau) = \int_0^\beta d\tau \langle T_\tau \frac{1}{2}(S_1^+(\tau) - S_2^+(\tau)) \frac{1}{2}(S_1^-(\tau) - S_2^-(\tau)) \rangle / 2$, with $S_i^- = d_{i\downarrow}^\dagger d_{i\uparrow}$ and $S_i^+ = S_i^-^\dagger$, such that $\chi_z = \chi_{+-}$ at the $I_z = 0$ SU(2)-symmetric point. The result is consistent with $\chi_{+-}(\tau) \sim 1/\tau^{1+y}$, with y taking the same value (within numerical uncertainty) as found in the singlet pairing susceptibility $\chi_d(\tau)$.

Appendix D: Additional data from NRG

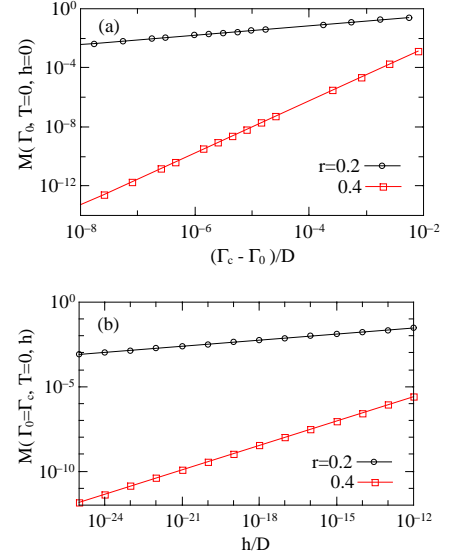


FIG. 10: (a) Staggered local moment $M(\Gamma_0, T = 0, h = 0)$ vs $\Gamma_c - \Gamma_0$, fitted to $M \propto (\Gamma_c - \Gamma_0)^{\beta'}$ with $\beta' = 0.31991(2)$ for $r = 0.2$ and $\beta' = 1.7701(2)$ for $r = 0.4$. (b) Staggered local moment $M(\Gamma_0 = \Gamma_c, T = 0, h)$ vs staggered external magnetic field h , fitted to $M \propto h^{1/\delta}$ with $1/\delta = 0.11990(4)$ for $r = 0.2$ and $1/\delta = 0.48066(4)$ for $r = 0.4$. Calculations are performed at $I_z = 1.54$ (0.73) for $r = 0.2$ (0.4).

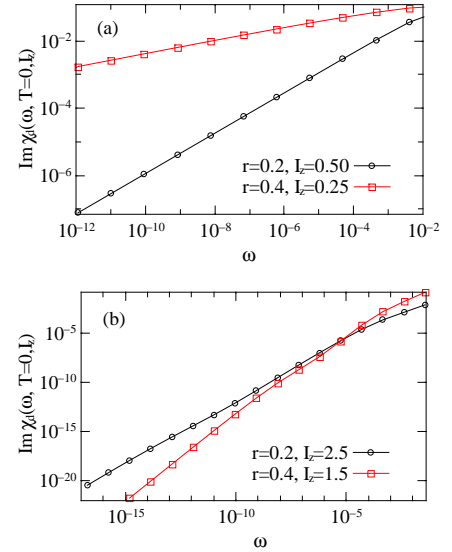


FIG. 11: $\text{Im} \chi_d(\omega)$ at $T = 0$ in (a) Kondo-screened and (b) local-moment phases. The low-frequency asymptotics give (a) $\text{Im} \chi_d(\omega) \text{sgn}(\omega) \propto |\omega|^{1-2r}$ and (b) $\text{Im} \chi_d(\omega) \text{sgn}(\omega) \propto |\omega|^{1+2r}$. Calculations are performed at $\Gamma_0 = 0.5503$ and $\Gamma_0 = 0.8032$, respectively.

Appendix E: Derivation of Eq. (8)

We make use of the Kramers-Kronig relation

$$\text{Re } \chi_d(\omega = 0) = \frac{1}{\pi} \int_{-\infty}^{\infty} d\omega' \frac{\text{Im } \chi_d(\omega')}{\omega'}. \quad (\text{E1})$$

Because $\text{Im } \chi_d(\omega')$ is odd,

$$\begin{aligned} & \text{Re } \chi_d(\omega = 0) \\ &= \frac{2}{\pi} \int_0^{\infty} d\omega \frac{\text{Im } \chi_d(\omega)}{\omega} \\ &= \frac{2}{\pi} \left(\int_0^{\omega^*} d\omega + \int_{\omega^*}^{\omega_1} d\omega + \int_{\omega_1}^{\infty} d\omega \right) \frac{\text{Im } \chi_d(\omega)}{\omega}, \quad (\text{E2}) \end{aligned}$$

where $\omega^* \sim |(I_z - I_c)/I_c|^\nu$ is the crossover scale into the quantum critical regime, and ω_1 is some upper cut-off, which we have assumed to be independent of I_z . The high-frequency non-universal part should only have a weak dependence on I_z , so we put $\int_{\omega_1}^{\infty} d\omega [\text{Im } \chi_d(\omega)]/\omega \simeq D_1(r)$.

Now we substitute Eq. (7) in the main text.

$$\begin{aligned} & \text{Re } \chi_d(\omega = 0) \\ &= \frac{2}{\pi} \int_0^{\omega^*} C \left(\frac{\omega^*}{D} \right)^y \left(\frac{\omega}{\omega^*} \right)^{1 \pm 2r} \frac{1}{\omega} d\omega \\ &+ \frac{2}{\pi} \int_{\omega}^{\omega_1} C \left(\frac{\omega^*}{D} \right)^y \frac{1}{\omega} d\omega + D_1(r) \\ &= \frac{2}{\pi} C \left(\frac{\omega^*}{D} \right)^y \frac{1}{1 \pm 2r} + \frac{2}{\pi} C \frac{1}{y} \frac{(\omega_1^y - \omega^{*y})}{D^y} + D_1(r) \\ &= \frac{2C}{\pi} \left[\frac{1}{y} \frac{\omega_1^y}{D^y} - \left(\frac{\omega^*}{D} \right)^y \left(\frac{1}{y} - \frac{1}{1 \pm 2r} \right) \right] + D_1(r) \quad (\text{E3}) \end{aligned}$$

From NRG data, the proportionality constant C has negligible dependence on I_z . Finally we replace ω^* by $|(I_z - I_c)/I_c|^\nu$ to obtain

$$\begin{aligned} & \text{Re } \chi_d(\omega = 0) \\ &= C_1(r) \\ &- C_2(r) \left(\frac{1}{y} - \frac{1}{1 \pm 2r} \right) \left(\frac{|(I_z - I_c)/I_c|^\nu}{D} \right)^y, \quad (\text{E4}) \end{aligned}$$

where

$$C_1(r) = \frac{2C(r)}{\pi} \frac{1}{y} \frac{\omega_1^y}{D^y} + D_1(r), \quad C_2(r) = \frac{2C(r)}{\pi}. \quad (\text{E5})$$

-
- ¹ P. A. Lee, N. Nagaosa, and X.-G. Wen, *Rev. Mod. Phys.* **78**, 17 (2006).
² Q. Si, R. Yu, and E. Abrahams, *Nat. Rev. Mater.* **1**, 16017 (2016).
³ Y. Takabayashi et al., *Science* **323**, 1585 (2009).
⁴ Q. Si and F. Steglich, *Science* **329**, 1161 (2010).
⁵ H. Löhneysen, A. Rosch, M. Vojta, and P. Wölfle *Rev. Mod. Phys.* **79**, 1015, (2007).
⁶ J. A. Hertz, *Phys. Rev. B* **14**, 1165 (1976).
⁷ A. J. Millis, *Phys. Rev. B* **48**, 7183 (1993).
⁸ T. Moriya *Spin Fluctuations in Itinerant Electron Magnetism*, **56**, 44–81 (Springer, 1985).
⁹ Q. Si, S. Rabello, K. Ingersent, and J. L. Smith, *Nature* **413**, 804 (2001).
¹⁰ P. Coleman, C. Pépin, Q. Si, and R. Ramazashvili, *J. Phys.: Condens. Matter* **13**, R723 (2001).
¹¹ T. Park, F. Ronning, H. Q. Yuan, M. B. Salamon, R. Movshovich, J. L. Sarrao, and J. D. Thompson, *Nature* **440**, 65 (2006).
¹² T. Park, E. D. Bauer, and J. D. Thompson *Phys. Rev. Lett.* **101**, 177002 (2008).
¹³ O. Stockert, S. Kirchner, F. Steglich, Q. Si, *J. Phys. Soc. Jpn.* **81**, 011001 (2012).
¹⁴ Q. Si, J. H. Pixley, E. Nica, S. J. Yamamoto, P. Goswami, R. Yu, and S. Kirchner, *J. Phys. Soc. Jpn.* **83**, 061005 (2014).
¹⁵ H. Shishido, R. Settai, H. Harima, and Y. Ōnuki, *J. Phys. Soc. Jpn.* **74**, 1103 (2005).
¹⁶ J. H. Pixley, S. Kirchner, K. Ingersent, and Q. Si, *Phys. Rev. B* **88**, 245111 (2013).
¹⁷ S. Kirchner and Q. Si, *Phys. Rev. Lett.* **100**, 026403 (2008).
¹⁸ J. H. Pixley, S. Kirchner, K. Ingersent, and Q. Si, *Phys. Rev. Lett.* **109**, 086403 (2012).
¹⁹ K. Ingersent and Q. Si, *Phys. Rev. Lett.* **89**, 076403 (2002).
²⁰ M. T. Glossop, S. Kirchner, J. H. Pixley, and Q. Si, *Phys. Rev. Lett.* **107**, 076404 (2011).
²¹ J. H. Pixley, A. Cai and Q. Si, *Phys. Rev. B* **91**, 125127 (2015).
²² J. H. Pixley, T. Chowdhury, M. T. Mieczkowski, J. Stephens, C. Wagner, and K. Ingersent, *Phys. Rev. B* **91**, 245122 (2015).
²³ J. H. Pixley, L. Deng, K. Ingersent, and Q. Si, *Phys. Rev. B* **91**, 201109(R) (2015).
²⁴ D. Withoff and E. Fradkin *Phys. Rev. Lett.* **64**, 1835 (1990).

- ²⁵ R. Bulla, T. Pruschke, and A. C. Hewson, *J. Phys.: Condens. Matter* **9**, 10463 (1997).
- ²⁶ C. Gonzalez-Buxton, and K. Ingersent, *Phys. Rev. B* **57**, 14254 (1998).
- ²⁷ In the absence of the pseudogap, our model exhibits a Kosterlitz-Thouless quantum phase transition between Kondo and Kondo-destroyed phases; see M. Garst, S. Kehrein, T. Pruschke, A. Rosch, and M. Vojta, *Phys. Rev. B* **69**, 214413 (2004), also N. Andrei, G. T. Zimányi, G. Schön, *Phys. Rev. B* **60**, R5125 (1999).
- ²⁸ I. Affleck and A. W. W. Ludwig, *Phys. Rev. Lett.* **68**, 1046 (1992); I. Affleck, A. W. W. Ludwig, and B. A. Jones, *Phys. Rev. B* **52**, 9528 (1995).
- ²⁹ J. Gan, *Phys. Rev. Lett.* **74**, 2583 (1995); *Phys. Rev. B* **51**, 8287 (1995).
- ³⁰ G. Zaránd, C. Chung, P. Simon, and M. Vojta, *Phys. Rev. Lett.* **97**, 166802 (2006).
- ³¹ P. Werner and A. J. Millis, *Phys. Rev. Lett.* **99**, 146404 (2007).
- ³² P. Werner and A. J. Millis, *Phys. Rev. Lett.* **104**, 146401 (2010).
- ³³ K. G. Wilson, *Rev. Mod. Phys.* **47**, 773 (1975).
- ³⁴ R. Bulla, T. A. Costi, and T. Pruschke, *Rev. Mod. Phys.* **80**, 395 (2008).
- ³⁵ K. Binder, *Z. Phys. B* **43**, 119 (1981).
- ³⁶ J. Houdayer and A. K. Hartmann, *Phys. Rev. B* **70**, 014418 (2004).
- ³⁷ For $r = 0.4$, sub-leading corrections to scaling are sufficiently strong that it proved challenging for CT-QMC to reproduce the NRG value of ν^{-1} within estimated error. We attained this goal by using NRG calculations to select the value $\Gamma_0 = 1.5$ that produces the highest temperature of entry into the quantum critical regime.
- ³⁸ M. Kirčan, and M. Vojta, *Phys. Rev. B* **69**, 174421 (2004).
- ³⁹ We note that in the infinite-separation limit, the pairing correlation of $d_{2\downarrow}d_{1\uparrow} + d_{2\uparrow}d_{1\downarrow}$ is degenerate with that of $d_{2\downarrow}d_{1\uparrow} - d_{2\uparrow}d_{1\downarrow}$.
- ⁴⁰ E. Gull, P. Werner, A. Millis, and M. Troyer, *Phys. Rev. B* **76**, 235123 (2007).